

Error Analysis of Variations on Larsen's Benchmark Problem

Y. Y. Azmy
Oak Ridge National Laboratory
P.O. Box 2008, MS-6363
Oak Ridge, Tennessee 37831-6363\
azmyyy@ornl.gov

Prepared for:

2001 ANS International Meeting on
Mathematical Methods for Nuclear Applications
September 9-13, 2001
Salt Lake City, Utah
USA

The submitted manuscript has been authored by a contractor of the U.S. Government under contract No. DE-AC05-00OR22725. Accordingly, the U.S. Government retains a nonexclusive, royalty-free license to publish or reproduce the published form of this contribution, or allow others to do so, for U.S. Government purposes.

ERROR ANALYSIS OF VARIATIONS ON LARSEN'S BENCHMARK PROBLEM

Y. Y. Azmy

Oak Ridge National Laboratory
P. O. Box 2008, MS 6363
Oak Ridge, Tennessee 37831-6363
azmyyy@ornl.gov

Keywords: Discrete Ordinates Transport, Diamond Difference Method, Nodal Methods, Characteristics Methods, Error Analysis.

ABSTRACT

Error norms for three variants of Larsen's benchmark problem are evaluated using three numerical methods for solving the discrete ordinates approximation of the neutron transport equation in multidimensional Cartesian geometry. The three variants of Larsen's test problem are concerned with the incoming flux boundary conditions: unit incoming flux on the left and bottom edges (Larsen's configuration); unit incoming flux only on the left edge; unit incoming flux only on the bottom edge. The three methods considered are the Diamond Difference (DD) method, and the constant-approximation versions of the Arbitrarily High Order Transport method of the Nodal type (AHOT-N), and of the Characteristic (AHOT-C) type. The cell-wise error is computed as the difference between the cell-averaged flux computed by each method and the exact value, then the L_1 , L_2 , and L_∞ error norms are calculated. The results of this study demonstrate that while integral error norms, i.e. L_1 , L_2 , converge to zero with mesh refinement, the pointwise L_∞ norm does not due to solution discontinuity across the singular characteristic. Little difference is observed between the error norm behavior of the three methods considered in spite of the fact that AHOT-C is locally exact, suggesting that numerical diffusion across the singular characteristic as the major source of error on the global scale. However, AHOT-C possesses a given accuracy in a larger fraction of computational cells than DD.

1 INTRODUCTION

Error analysis of the numerical methods employed in deriving discrete-variable formulations for solving the multidimensional neutron transport equation have long established their suitability. The multigroup approximation of the energy dependence

was shown to converge to the exact solution with refinement of the energy group structure if the fluctuations in the total and scattering cross sections diminish with refinement of the energy group structure (Victory, 1985).

Madsen (1971) proved convergence of the discrete ordinates method solution to the exact solution of the continuum angle, monoenergetic transport equation provided the scattering ratio is smaller than 1, and decreasing error in the quadrature formula with increasing angular quadrature order. Then Madsen (1972) also proved convergence of the Diamond Difference (DD) method solution to the discrete ordinates approximation of the monoenergetic, multidimensional transport equation; however, the value of the proof is questionable because it requires the continuity of the exact solution. Later Madsen (1973) derived L_1 and L_2 *a posteriori* error bounds on numerical solutions to the multidimensional neutron transport equation but this time requiring only that the exact solution be absolutely continuous almost everywhere. Still, this did not prove pointwise convergence, or even convergence in a norm sense with mesh refinement, and it is not clear whether relaxing the continuity requirement in (Madsen, 1972) to *almost everywhere* will correctly settle this question.

The above results, among others, are based on rigorous mathematical analysis and yielded proofs of solution convergence in one or more norms that can be used to set an upper bound on the error in the solution related to the discretization parameters in each of the independent variables. Important as this may be, it rarely produces sufficiently tight error bounds that are useful in practical applications. Hence, many works were published that aimed at quantifying the solution error for various methods via numerical experiments on specific, typically simple problem configurations, and assuming that the observed behavior extends to other more complex practical applications. Clearly this approach is not rigorous, nevertheless it produces useful information, namely explicit values of the error on a per computational cell basis.

This paper examines one such simple monoenergetic, single discrete ordinate configuration proposed by Larsen (1982) to study the solution convergence properties of numerical methods employed in solving the discrete ordinate approximation of the neutron transport equation. Larsen (1982) determined the convergence rate of the L_1 , L_2 , and L_∞ error norms of the DD method and found that all three approached zero with mesh refinement in fractional powers of the computational cell size. More recently, a local error analysis of DD, among other methods, implied lack of convergence of the solution to the exact local solution, with diminishing cell size, when the incoming edge fluxes are not equal (Azmy, 2000).

The main goal of this work is to reconcile these seemingly contradictory conclusions and put them in perspective with earlier rigorous analyses, particularly (Madsen, 1972). In Sec. 2 we briefly review the local error analysis of WDD methods

and determine the asymptotic order of the local error as a function of cell size for fixed cell optical aspect ratio. Expressions for the exact cell-averaged flux in Larsen's benchmark problem are derived in Sec. 3 for the benefit of determining the cell-wise error. The cell-averaged flux obtained by DD, and the lowest order approximation of AHOT-N, and of AHOT-C are used in Sec. 4 to compute and compare the global error for each of these methods. Our conclusions from this exercise are summarized in Sec. 5.

2 LOCAL ERROR ANALYSIS

A local error analysis of the Step method, and a class of Weighted Diamond Difference (WDD) methods, that includes as special cases the DD, and AHOT-N lowest order methods, has been presented recently for two-dimensional Cartesian geometry (Azmy, 2000). By *local* we mean the error in the cell-averaged and outgoing edge-averaged angular flux values assuming exact incoming edge-averaged angular flux, and cell averaged distributed source values.

Consider a rectangular computational cell of width $2a$ and height $2b$, and homogeneous material composition represented by the macroscopic total cross section, σ , and without any loss of generality consider a discrete ordinate in the first quadrant of angular space, $\mu, \eta > 0$. It is possible to exactly compute the contribution to the cell-averaged flux from three regions within the cell defined by the incoming corner and the discrete ordinate angle under consideration. This is accomplished by using the method of characteristics to derive an expression for the flux at an arbitrary point within the cell in terms of the incoming edge fluxes, i.e. the bottom-, and left-edge fluxes, ψ_B , and ψ_L , respectively, and the effective distributed source, \bar{S} . For the purpose of the lowest order spatial approximation considered here these quantities are assumed constant; they are also assumed to be exact by virtue of the local analysis conducted here. The resulting space dependent expression for the angular flux is then averaged over the cell volume to produce the cell-averaged flux, $\bar{\Psi}$, then over the length of each outgoing edge to produce the outgoing edge-averaged angular fluxes on the right, and top edges, Ψ_R , and Ψ_T , respectively,

$$\begin{aligned} \bar{\Psi} = & \left[\frac{e^{-\epsilon_y}}{\epsilon_x} + \left(\frac{1 - e^{-\epsilon_y}}{\epsilon_y} \right) \left(1 - \frac{1}{\epsilon_x} \right) \right] \psi_B + \frac{1}{\epsilon_x} \left[1 - \frac{1 - e^{-\epsilon_y}}{\epsilon_y} \right] \psi_L \\ & + \left[1 - \frac{1 - e^{-\epsilon_y}}{\epsilon_y} - \frac{1 + e^{-\epsilon_y}}{\epsilon_x} + 2 \left(\frac{1 - e^{-\epsilon_y}}{\epsilon_x \epsilon_y} \right) \right] \frac{\bar{S}}{\sigma}, \end{aligned} \quad (1a)$$

$$\Psi_T = e^{-\epsilon_y} (1 - \xi) \psi_B + \frac{1 - e^{-\epsilon_y}}{\epsilon_x} \psi_L + \left[1 - e^{-\epsilon_y} (1 - \xi) - \frac{1 - e^{-\epsilon_y}}{\epsilon_x} \right] \frac{\bar{S}}{\sigma}, \quad (1b)$$

$$\Psi_R = \frac{1 - e^{-\epsilon_y}}{\epsilon_y} \psi_B + \left(1 - \frac{1 - e^{-\epsilon_y}}{\epsilon_y} \right) \frac{\bar{S}}{\sigma}. \quad (1c)$$

In Eqs. (1) we defined the cell optical dimensions $\epsilon_x \equiv (2\sigma a)/\mu$, $\epsilon_y \equiv (2\sigma b)/\eta$, and the cell optical aspect ratio $\xi \equiv \epsilon_y/\epsilon_x$; without any loss of generality we assume $0 < \xi \leq 1$.

The WDD equations in the same computational cell include a balance equation, a weighted difference relation in the x -dimension, and one in the y -dimension

$$\frac{\psi_R - \psi_L}{\epsilon_x} + \frac{\psi_T - \psi_B}{\epsilon_y} + \bar{\psi} = \bar{S}/\sigma, \quad (2a)$$

$$\bar{\psi} = \frac{1 + \alpha_x}{2} \psi_R + \frac{1 - \alpha_x}{2} \psi_L, \quad (2b)$$

$$\bar{\psi} = \frac{1 + \alpha_y}{2} \psi_T + \frac{1 - \alpha_y}{2} \psi_B, \quad (2c)$$

respectively, where $\alpha_u \in [0, 1]$ is the spatial weight in the $u \equiv x, y$ dimension. The selection of the spatial weights determines a specific WDD scheme; $\alpha_u = 0$ is DD, $\alpha_u = 1$ is the Step Method (SM), and $\alpha_u = \coth(\epsilon_u/2) - 2/\epsilon_u$ is the lowest order Nodal Integral Method (AHOT-N0).

By solving the WDD equations for the cell-averaged flux, $\bar{\psi}$, and the outgoing edge-averaged angular fluxes on the right, and top edges, ψ_R and ψ_T , respectively, as a function of \bar{S}/σ , ψ_L and ψ_B , as well as the parameters ϵ_x , α_x , ϵ_y , and α_y , the error is computed as the difference from the exact solution represented by Eqs. (1). It has been shown that when the incoming fluxes are not equal, hence the exact solution is discontinuous across the characteristic line subtended from the lower left corner, the numerical method solutions do not converge to the exact solution as the cell size approaches zero, i.e. $\epsilon_x \rightarrow 0$, $\xi = \text{const}$. In contrast, when the incoming edge fluxes are equal, hence the solution is continuous but not smooth, across the characteristic, the numerical methods solutions converged like $O(\epsilon_x)$. Clearly these conclusions do not apply to characteristic methods, e.g. AHOT-C, since these are constructed from the exact local solution to the transport equation.

Further insight into the lack of convergence of the WDD-computed cell-averaged flux to its exact value is gained by determining the asymptotic behavior of the exact and numerical methods solutions with diminishing cell size. Hence introducing $\epsilon_y \equiv \xi \epsilon_x$ and $\epsilon_x \rightarrow 0$ in Eq. (1) yields

$$\bar{\Psi} \rightarrow \left(1 - \frac{\xi}{2}\right) \psi_B + \frac{\xi}{2} \psi_L + O(\epsilon_x). \quad (3)$$

Solving the WDD equations simultaneously, then taking the same limits in the

expression for $\bar{\psi}$ results in

$$\bar{\psi} \rightarrow \left[1 + \xi \left(\frac{1 + \alpha_y}{1 + \alpha_x} \right) \right]^{-1} \psi_B + \left[1 + \frac{1}{\xi} \left(\frac{1 + \alpha_x}{1 + \alpha_y} \right) \right]^{-1} \psi_L + O(\epsilon_x). \quad (4)$$

A few observations follow from Eqs. (3) and (4). First we note that the dependence of the cell-averaged flux, both exact and approximate, on the distributed source is $O(\epsilon_x)$ while its dependence on the incoming edge-averaged flux is $O(1)$. Second, the difference between the asymptotic expressions for the exact and approximate cell-averaged fluxes does not vanish in general as $\epsilon_x \rightarrow 0$, as predicted previously, (Azmy, 2000). Third, for WDD methods with weights $\alpha_x, \alpha_y \rightarrow 0$ as $\epsilon_x, \epsilon_y \rightarrow 0$, such as DD and AHOT-N0 the local error vanishes like $O(\epsilon_x)$ if $\psi_B = \psi_L$, again as observed earlier (Azmy, 2000).

3 EXACT CELL-WISE SOLUTION

Larsen's benchmark problem was designed to have a simple configuration for which an analytical solution can be easily determined and used to compute the convergence order of the DD cell-averaged flux error with mesh refinement (Larsen, 1982). The problem domain is a rectangular region of dimensions $X \times Y$, containing a non-scattering material and no distributed fixed source. Only one discrete ordinate, $\mu, \eta > 0$, is considered, and since the scattering ratio is zero the scalar flux is a fixed fraction of the angular flux in this direction. Constant incoming flux is defined on the left and bottom boundaries, and the analysis was confined to the case $\psi_L = 1 = \psi_B$. In view of the results presented in Sec. 2, the dominating role that the incoming edge-averaged flux discontinuity plays in determining the local error becomes evident and must be considered in any further analysis. Hence in this work we relax this condition.

A sequence of uniform meshes is then imposed on the problem domain, each mesh characterized by the integer n such that the number of computational cells in the x , and y dimensions is 2^n . It follows that for mesh n the computational cell size is $\delta_x \times \delta_y \equiv X/2^n \times Y/2^n$, and its optical dimensions become $\epsilon_x \times \epsilon_y \equiv X/(2^n \mu) \times Y/(2^n \eta)$. The exact solution to this problem is given by

$$\psi(x, y) = \begin{cases} \psi_B e^{-y/\eta} & y < x\eta/\mu \\ \psi_L e^{-x/\mu} & y > x\eta/\mu \end{cases} \quad (5)$$

The solution is not defined along the singular characteristic (SC), $x/\mu = y/\eta$, since it could experience a discontinuity across it.

Larsen (1982) computed the error as the difference between the DD solution, i.e. cell-averaged flux values, and the exact point values at cell centers obtained with

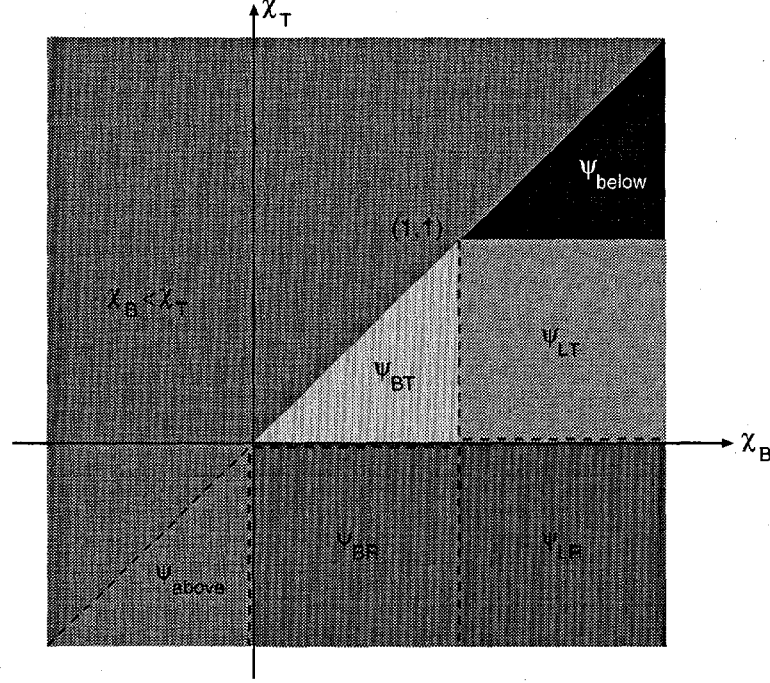


Fig. 1. Possible Intersection of SC with Cell Edges Over the (χ_B, χ_T) -plane

the analogue of Eq. (5), correctly arguing that the difference will not change the order of convergence. In order to improve the fidelity of the global error analysis conducted in Sec. 4, in this section we develop exact formulas for the cell-averaged flux over individual cells using the exact solution, Eq. (5). Clearly such formula will depend on the positional relationship of the cell with respect to the SC, which can be quantified by the intersection of SC with the bottom and top edges of the computational cell. In particular, consider cell i, j whose center lies at $([i-1/2] \delta_x, [j-1/2] \delta_y)$ and whose four corners have coordinates $([i-1] \delta_x, [j-1] \delta_y)$, $(i \delta_x, [j-1] \delta_y)$, $(i \delta_x, j \delta_y)$, $([i-1] \delta_x, j \delta_y)$ ordered counter-clockwise starting from the lower left corner. Denote the coordinates of the intersection points of the SC with the bottom, and top edges of this cell with $([i - \chi_B] \delta_x, [j - 1] \delta_y)$, and $([i - \chi_T] \delta_x, j \delta_y)$, respectively, where

$$(i - \chi_B) \delta_x = \frac{\mu}{\eta} (j - 1) \delta_y \Rightarrow \chi_B = i - (j - 1) \frac{\epsilon_y}{\epsilon_x}, \quad (6a)$$

$$(i - \chi_T) \delta_x = \frac{\mu}{\eta} j \delta_y \Rightarrow \chi_T = i - j \frac{\epsilon_y}{\epsilon_x} = \chi_B - \frac{\epsilon_y}{\epsilon_x}. \quad (6b)$$

If the SC intersects the bottom edge, then $\chi_B \in [0,1]$, attaining the values 0, and 1 on the right, and left lower corners of the cell, respectively. Analogously, if the SC intersects the top edge, then $\chi_T \in [0,1]$, attaining the values 0, and 1 on

the right, and left upper corners of the cell, respectively. Since $\chi_B > \chi_T$ by Eq. (6b), it follows that the SC does not intersect the cell at all if $\chi_B < 0$, or $\chi_T > 1$, where the cell lies entirely above, or below the SC, respectively. There is a total of six possible combinations of χ_B and χ_T satisfying $\chi_B > \chi_T$ that must be considered separately. These are depicted in Fig. 1 in color-code on the χ_B, χ_T plane: the *above* and *below* subscripts refer to the two cases listed above; the other subscripts refer to the edges intersected by the SC with B, R, T, L, denoting bottom, right, top, and left, edges respectively. Edges are assigned to regions in the χ_B, χ_T plane as depicted in the figure; the color within the dashed lines marks the region to which an edge is assigned.

Finally, integrating the exact solution, Eq. (5), over cell i, j in each of the six valid regions shown in Fig. 1 yields the expressions

$$\psi_{above} = \frac{e^{-i\epsilon_x}}{\epsilon_x} (e^{\epsilon_x} - 1) \psi_L, \quad (7a)$$

$$\psi_{below} = \frac{e^{-j\epsilon_y}}{\epsilon_y} (e^{\epsilon_y} - 1) \psi_B, \quad (7b)$$

$$\begin{aligned} \psi_{BR} &= \frac{1}{\epsilon_x \epsilon_y} [e^{-i\epsilon_x} \{\epsilon_y \psi_L (e^{\epsilon_x} - \zeta_R) + \psi_B (1 - e^{\chi_B \epsilon_x})\} \\ &+ e^{-j\epsilon_y} \{\psi_L (e^{\zeta_R \epsilon_y} - e^{\epsilon_y}) + \chi_B \epsilon_x e^{\epsilon_y} \psi_B\}], \end{aligned} \quad (7c)$$

$$\begin{aligned} \psi_{LT} &= \frac{1}{\epsilon_x \epsilon_y} [e^{-j\epsilon_y} \{\epsilon_x \psi_B (e^{\epsilon_y} - \chi_T) + \psi_L (1 - e^{\zeta_L \epsilon_y})\} \\ &+ e^{-i\epsilon_x} \{\psi_B (e^{\chi_T \epsilon_x} - e^{\epsilon_x}) + \zeta_L \epsilon_y e^{\epsilon_x} \psi_L\}], \end{aligned} \quad (7d)$$

$$\begin{aligned} \psi_{BT} &= \frac{e^{-i\epsilon_x}}{\epsilon_x} \left[e^{\epsilon_x} \psi_L + \frac{e^{\chi_T \epsilon_x} - e^{\chi_B \epsilon_x}}{\epsilon_y} \psi_B \right] \\ &+ \frac{e^{-j\epsilon_y}}{\epsilon_y} \left[\frac{1 - e^{\epsilon_y}}{\epsilon_x} \psi_L + (\chi_B e^{\epsilon_y} - \chi_T) \psi_B \right], \end{aligned} \quad (7e)$$

$$\begin{aligned} \psi_{LR} &= \frac{e^{-j\epsilon_y}}{\epsilon_y} \left[e^{\epsilon_y} \psi_B + \frac{e^{\zeta_R \epsilon_y} - e^{\zeta_L \epsilon_y}}{\epsilon_x} \psi_L \right] \\ &+ \frac{e^{-i\epsilon_x}}{\epsilon_x} \left[\frac{1 - e^{\epsilon_x}}{\epsilon_y} \psi_B + (\zeta_L e^{\epsilon_x} - \zeta_R) \psi_L \right], \end{aligned} \quad (7f)$$

where the intercept parameters ζ_L and ζ_R are defined in analogy to χ_B and χ_T .

The above expressions are used in Sec. 4 to generate color-coded plots of the exact solution to Larsen's benchmark problem, and of the cell-wise error. Also presented in Sec. 4 are solutions and error values for the locally exact, lowest order

approximation of AHOT-C (AHOT-C0) whose equations for cell i, j are the same as Eqs. (1).

4 GLOBAL ERROR ANALYSIS

The original work on Larsen's benchmark problem set the rectangular domain dimensions at $X \times Y = 1.3 \times .9 \text{ mfp}$, and considered the source free case, $\bar{S} = 0$ (Larsen, 1982). In light of the asymptotic analysis presented in Sec. 2, i.e. Eqs. (3) and (4), this setting of the distributed source does not influence the order of the error in cases with discontinuous incoming edge-averaged flux. The lack of scattering causes the angular fluxes to be completely decoupled, hence the error in only one direction, $\mu = .7 = \eta$, need be considered. The sequence of uniform meshes described earlier, $X 2^{-n} \times Y 2^{-n}$, is applied to the rectangular region and numerical solutions are obtained for the cell-averaged flux using WDD with the spatial weights set to select either the DD or AHOT-N0. Also Eqs. (1) are used to obtain the AHOT-C0 cell-averaged flux, and Eqs. (7) are used to compute the exact cell-averaged flux distribution.

Three cases are considered in the analysis: $\psi_L = 0, \psi_B = 1$; $\psi_L = 1, \psi_B = 0$; and the case considered by Larsen (1982) $\psi_L = 1, \psi_B = 1$. For each of these cases we compute, in 64-bit arithmetic, the exact and numerical methods solutions, then compute the error distribution as the difference between these quantities. The error distribution is then used to calculate L_1, L_2 , and L_∞ norms for each considered method, and each choice of the boundary conditions. The error norms for the DD and AHOT-C0 methods and the case $\psi_L = 1, \psi_B = 1$ are shown in Fig. 2; the plots include the error norm for each considered mesh, i.e. $-n = -15, \dots, 0$, as well as the asymptotic behavior of each error norm. The latter is plotted as a straight line (in the log scale employed) emanating from each norm's error point at $n=15$ with gradient $-\log(\varepsilon_{\ell,15}/\varepsilon_{\ell,14})$, where $\varepsilon_{\ell,n}$ is the L_ℓ error norm, $\ell = 1, 2, \infty$. The computed asymptotic rate of convergence of each error norm for this case is provided in Table 1. The DD results shown in Fig. 2 and Table 1 are consistent with Larsen's (1982). In essence, both the DD (by implication AHOT-N0 also) and AHOT-C0 solutions converge to the exact cell-wise solution with mesh refinement in all three norms. It is surprising, however, that in spite of the locally exact nature of AHOT-C0 its solution error is larger than the WDD schemes.

Analogous error norm plots for the case $\psi_L = 0, \psi_B = 1$ are presented in Fig. 3, and the asymptotic convergence rates are presented in Table 2. The effect of solution discontinuity across the SC is evident in this case in more than one way. First, pointwise convergence of the solution is not achieved by any of the methods as evidenced by the L_∞ error norm. Second, all three error norms deteriorate significantly from the $\psi_L = 1, \psi_B = 1$ case where the solution is continuous across the

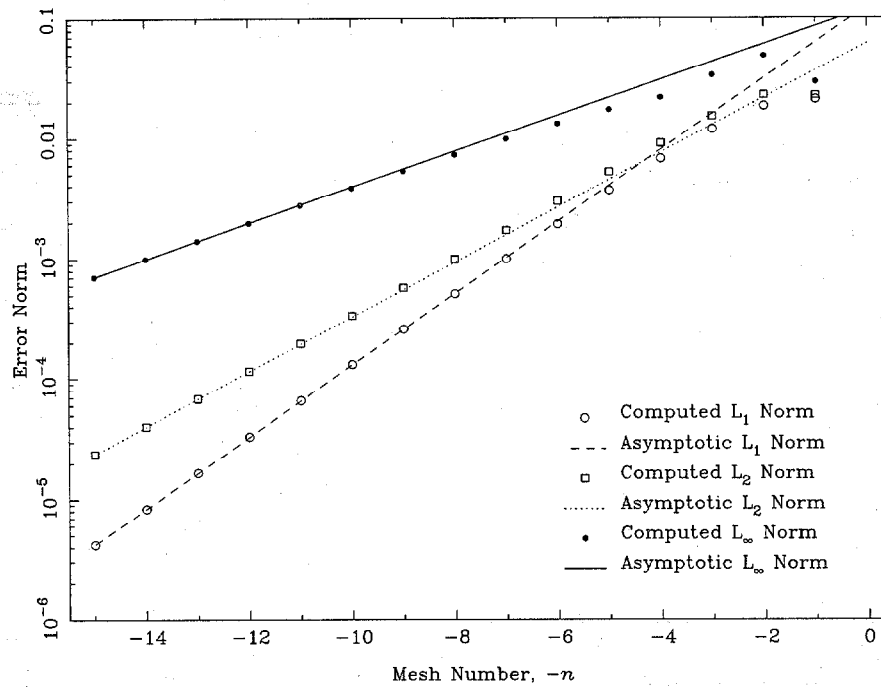
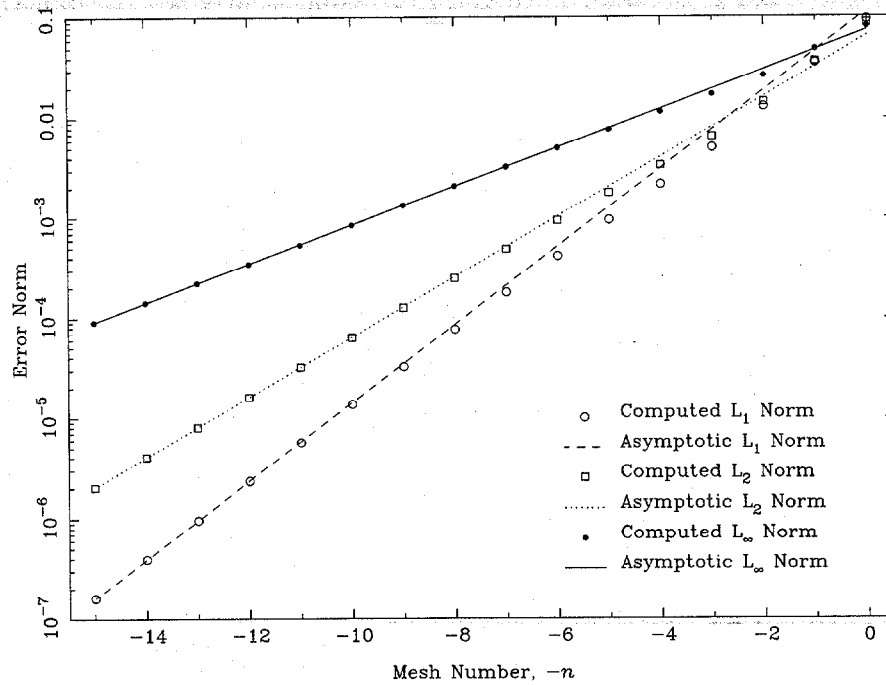


Fig. 2. Error Norms in the Cell-Averaged Fluxes Computed by the DD (Top) and AHOT-C0 (Bottom) Methods as the Mesh is Refined for the Case $\psi_L = 1$, $\psi_B = 1$.

SC. Finally, the AHOT-C0 error norms are not consistently worse than their WDD counterparts.

Table 1. Asymptotic Rate of Convergence of Error Norms for DD, AHOT-N0, and AHOT-C0 Solutions for the Case $\psi_L = 1$, $\psi_B = 1$.

Method	L_1	L_2	L_∞
DD	1.29517	0.99824	0.64461
AHOT-N0	1.28863	0.99720	0.64524
AHOT-C0	0.98986	0.75573	0.49406

Table 2. Asymptotic Rate of Convergence of Error Norms for DD, AHOT-N0, and AHOT-C0 Solutions for the Case $\psi_L = 0$, $\psi_B = 1$.

Method	L_1	L_2	L_∞
DD	0.47618	0.32073	-0.04297
AHOT-N0	0.47304	0.31716	-0.04307
AHOT-C0	0.49703	0.24389	-0.03016

How general these observations are, and what they translate into in real applications with scattering and geometric detail is not immediately evident from the results presented in this work. What is evident, though, is that flux discontinuity has a detrimental effect on solution accuracy as predicted by the local error analysis of Sec. 2. The L_1 and L_2 norms indicate that the adverse effect of flux discontinuity is local, and with mesh refinement its locale gets narrower and narrower, in agreement with Madsen's (1973) hypothesis and result; this is further verified by plots below.

One of the advantages deterministic methods have over Monte Carlo methods is that they naturally produce solution distributions over the problem domain, often a valuable piece of information for the user. Hence accuracy in the integral norm sense offered by the L_1 and L_2 norms does not provide a good tool for judging these methods in this respect. Color-coded plots of the exact, DD, and AHOT-C0 cell-averaged fluxes over the x, y -plane are illustrated in Fig. 4 with $n=4, 6, 8$, and 10, for the case $\psi_L = 0$, $\psi_B = 1$. The plots of the flux in Fig. 4 illustrate an interesting difference between the DD and AHOT-C0 solutions. The solution discontinuity causes ripples in the DD solution surface below the SC that damp away within a band that diminishes in size with mesh refinement. In contrast, the AHOT-C0 solution is highly accurate below the diagonal joining the lower-left corner to the upper-right corner; it suffers its worst error, a smearing of the sharp edge of the flux discontinuity, in a tight band around the SC.

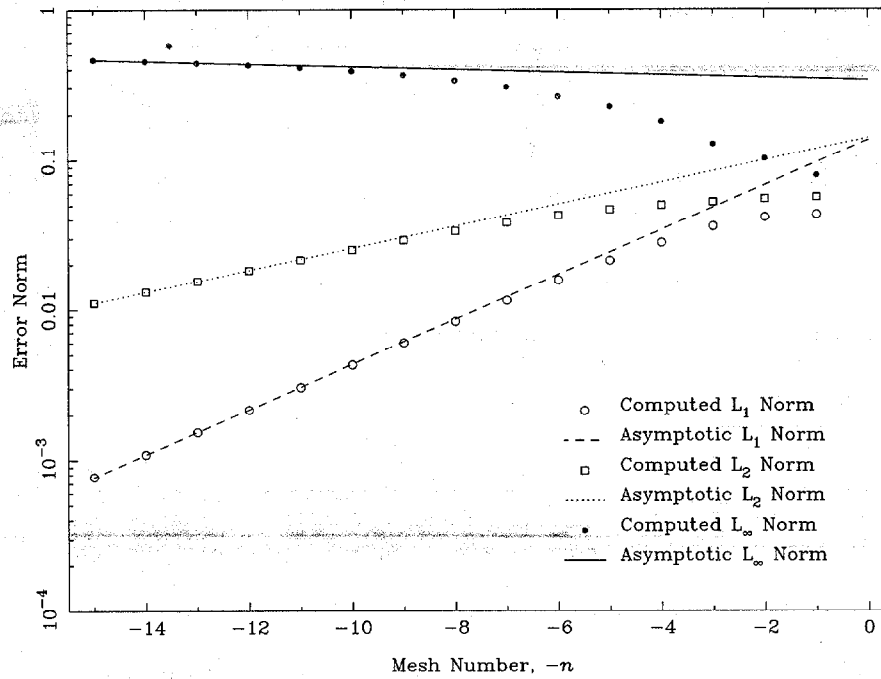
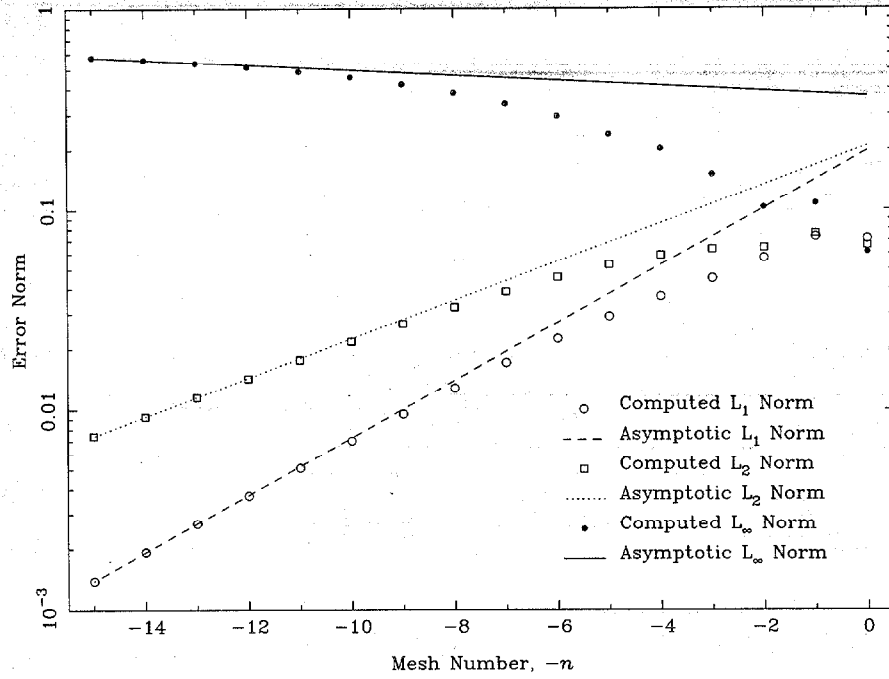


Fig. 3. Error Norms in the Cell-Averaged Fluxes Computed by the DD (Top) and AHOT-C0 (Bottom) Methods as the Mesh is Refined for the Case $\psi_L = 0$, $\psi_B = 1$.

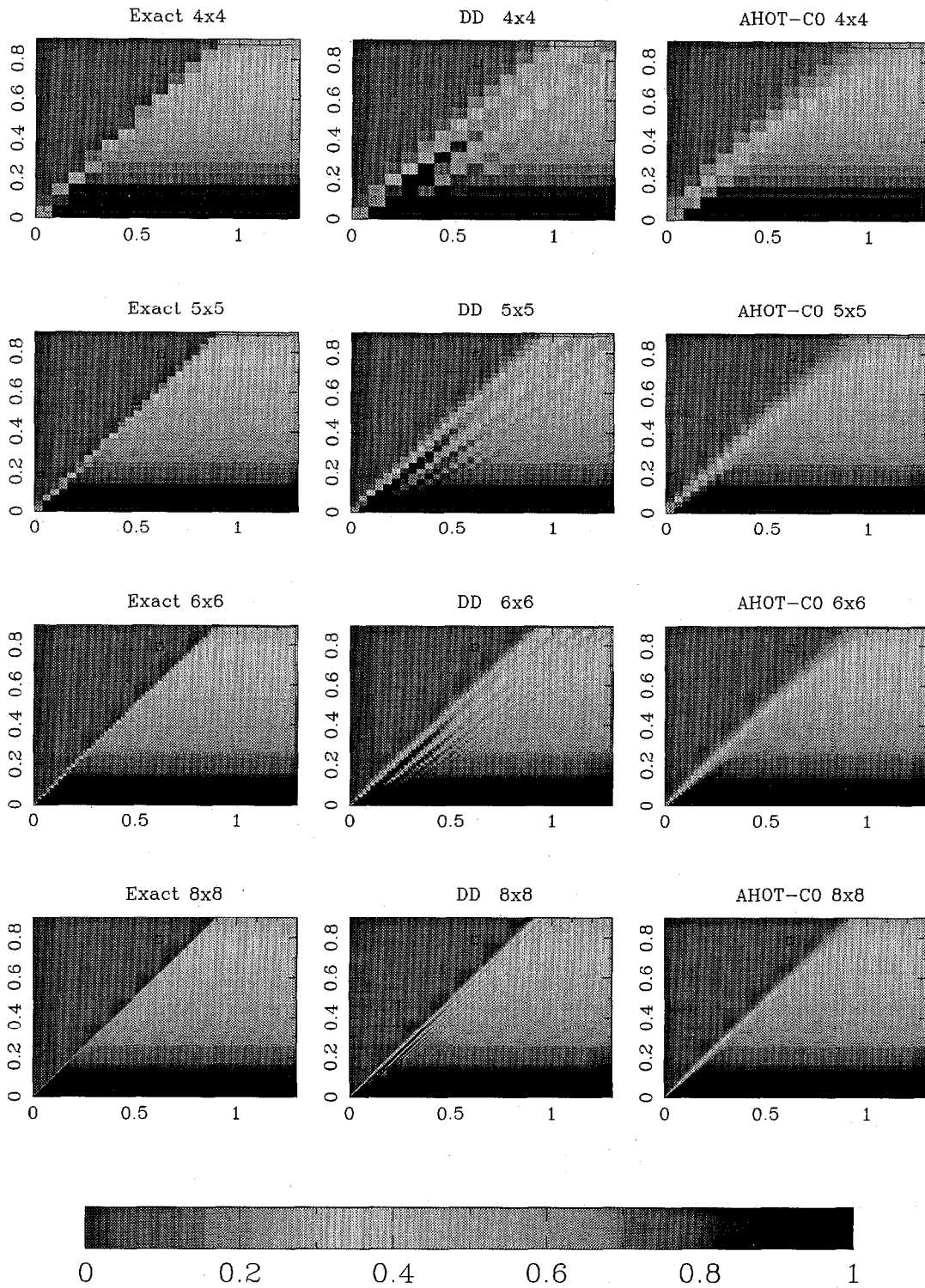


Fig. 4. Color-coded Plots of the Exact, DD, and AHOT-C0 Cell-Averaged Flux with $n=4, 5, 6,$ and $8,$ for the Case $\psi_L = 0, \psi_B = 1.$

The corresponding solution error distribution for the DD and AHOT-C0 methods, computed as the difference between each method's cell-averaged flux and the exact cell-averaged flux by cell is illustrated as color-coded plots in Fig. 5. Since the AHOT-N0 equations approach the DD equations in the fine mesh limit, their solutions are visually identical for sufficiently high n ; hence plots of the AHOT-N0 solution are not shown in Figs. 4 and 5.

Another way to look at the pointwise accuracy of numerical solutions is to examine the fraction of the number of cells as a function of error in the cell-averaged flux. This is depicted in Fig. 6 for the case $\psi_L = 0$, $\psi_B = 1$ solution of the DD, and AHOT-C0 methods, with $n=9$, 12, and 15. These plots indicate that the fraction of cells with smaller cell-averaged flux error increases with mesh refinement for both methods, but, in general, AHOT-C0 produces a larger fraction of cells where the solution is highly accurate than does the DD method.

5 CONCLUSION

We examined variants of Larsen's benchmark problem that introduce solution discontinuity across the singular characteristic via unequal incoming edge-averaged fluxes. We derived exact formulas for the cell-averaged flux on a uniform mesh covering the rectangular region comprising Larsen's benchmark problem, but with arbitrary incoming edge-averaged fluxes and used them to determine cell-wise errors and error norms for the DD, AHOT-N0, and AHOT-C0 methods. Local error analysis of WDD methods, including DD and AHOT-N0, indicates that the solutions do not converge to the locally exact value with diminishing cell size if the incoming edge-averaged fluxes are not equal. Indeed the cell-wise results confirm this behavior along the SC; the WDD solution converges with mesh refinement away from the SC because the inequality of the incoming edge-averaged fluxes diminishes for each computational cell.

The large error in the locally exact AHOT-C0 method solutions leads us to conjecture that it is dominated by numerical diffusion that tends to smear the sharp edge of the solution discontinuity over outgoing edges. In fact the similar error values observed for all three methods with mesh refinement in the cases with solution discontinuity leads us to further conjecture that the cell-averaged flux error is dominated by numerical diffusion effects, rather than local error effects, in general. This might add credence to high order methods that attempt to improve the flux representation on cell edges.

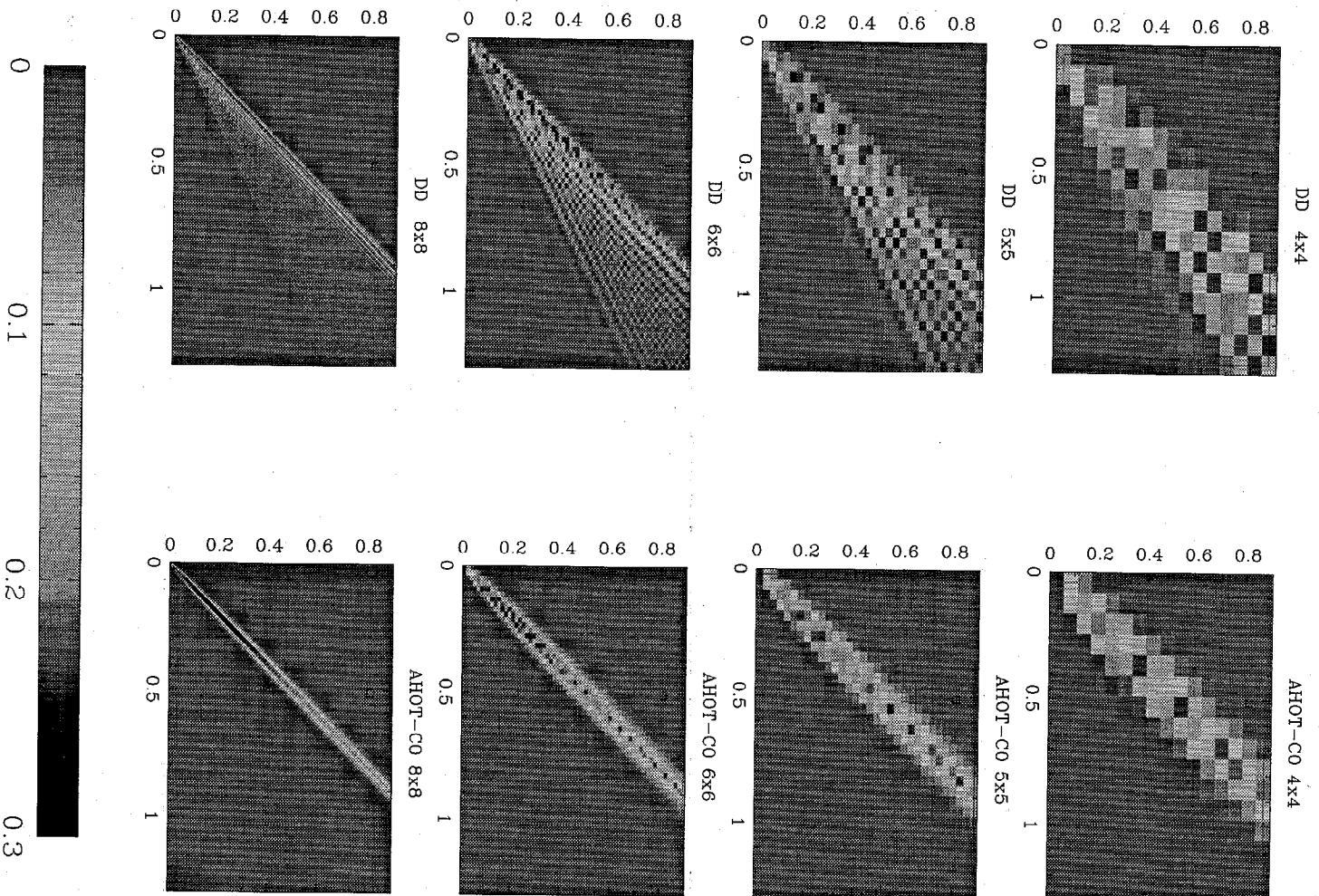


Fig. 5. Color-coded Plots of the DD, and AHOT-C0 Error in the Cell-Averaged Flux with $n=4, 5, 6,$ and $8,$ for the Case $\psi_L = 0, \psi_B = 1.$

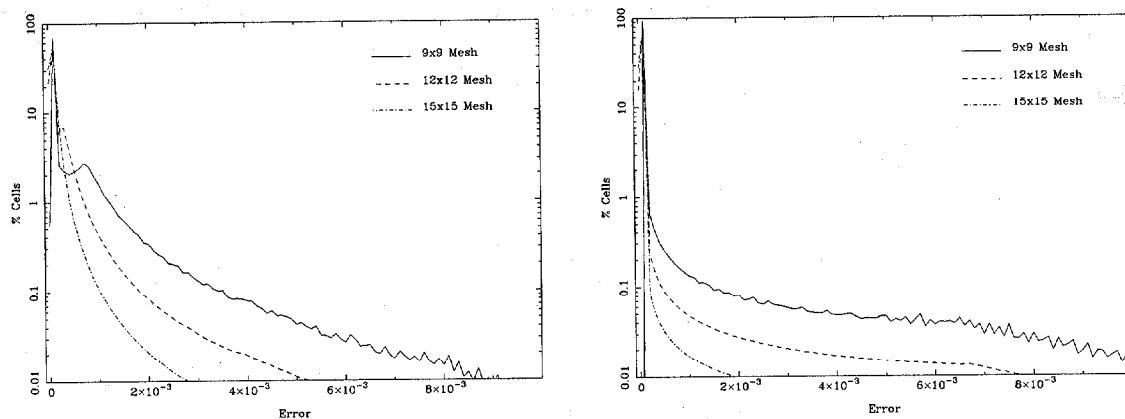


Fig. 6. Fraction of Cells *vs* Cell-Averaged Flux Error for the DD (Left), and AHOT-C0 (Right) with $n=9, 12,$ and $15,$ for the Case $\psi_L = 0, \psi_B = 1.$

References

- Victory, Jr., H. D., 1985. On the Convergence of the Multigroup Approximations for Multidimensional Media. *Annali di Matematica* **14**, 179.
- Madsen, N. K., 1971. Pointwise Convergence of the Three-Dimensional Discrete Ordinates Method. *SIAM J. Numer. Anal.* **8**, 266.
- Madsen, N. K., 1972. Convergence of Singular Difference Approximations for the Discrete Ordinate Equation in $x - y$ Geometry. *Mathematics of Computation* **26**, 45.
- Madsen, N. K., 1973. A Posteriori Error Bounds for the Numerical Solutions of the Neutron Transport Equation. *Mathematics of Computation* **27**, 773.
- Larsen, E. W., 1982. Spatial Convergence Properties of the Diamond Difference Method in x,y Geometry. *Nucl. Sci. Eng.* **80**, 710.
- Azmy, Y. Y., 2000. Local Accuracy of Weighted Diamond Difference Schemes. *Trans. Am. Nucl. Soc.* **83**, 433.

